Quantification of physical soil crust thickness and its effects on runoff and sediment yield

Abstract

Physical soil crusts will form on most soils during and after rainfall and it has important effects on the runoff and sediment on slopes. However, objective and effective methods for quantifying the characteristics of physical soil crusts (such as the thickness) are not currently available. We used a new method for determining the thickness of physical soil crusts based on X-ray computed tomography (CT) in order to quantify the thickness of the structural crust (SC) and depositional crust (DC) for two typical erosive soils comprising granite red soil (GRS) and Quaternary red clay (QRC) in the red soil region of southern China. The pores in the GRS and QRC were characterized as finely and densely spatially distributed, with an average porosity of 15.47% and a range of 1.66–28.83%. The soil porosity increased rapidly in the 0–3 mm depth, but the porosity of the SC and DC soil samples generally decreased or was stable in the 3–30 mm depth. The average thickness of the soil crust was 1.31 mm, and the average thicknesses of SC and DC were 1.16 and 1.46 mm, respectively. The thickness of SC of GRS decreased with the slope, whereas the thickness of DC of QRC generally increased with the slope. The thickness of SC increased with runoff yield and its contribution rate to the runoff cannot be neglected. The study provides a method for the objective quantification of physical soil crust and can deepen the research on slope erosion process and influencing factors.

Keywords: physical soil crust; red soil region; runoff and sediment yield; X-ray computed tomography

1. Introduction

A soil crust is a special structure that forms on the soil surface under different actions, which can significantly change soil hydrology and erosion processes, including evaporation, infiltration, runoff, and sediment yield (Armenise et al., 2018; Gao et al., 2017). Soil crusts are usually classified according to two categories comprising biological and physical soil crusts.

A biological soil crust is a complex formed of bryophytes, lichens, algae, bacteria, and fungi where mycelia, pseudoroots, and exudates are cemented with the underlying soil particles, so the surface soil is physically, chemically, and biologically distinct from the subsoil (Gao et al., 2017). A physical soil crust comprises a structural crust (SC) and depositional crust (DC) according to the formation process. SC is formed by raindrops hitting the soil surface and breaking aggregates, scattering fine particles, and blocking the pores in the topsoil. DC is formed via the deposition of fine particles carried in the overland flow on the soil surface (Lu et al., 2017). The formation processes differ for the two crusts but they are both dense soil structures, with important impacts on soil hydrology and erosion processes (Bu et al., 2014; Hu et al., 2005a; Wu et al., 2016).

Biological soil crusts have been studied extensively in terms of their formation process, surface structure and morphology, changes in the soil properties, impacts on hydrological processes and soil erosion, and other characteristics (Chamizo et al., 2012; Gao et al., 2017; Liu et al., 2016; Rodríguez-Caballero et al., 2015). However, studies on physical soil crusts were mainly focused on quantifying the properties of crusts and their impacts on soil hydrological processes, and runoff and sediment processes (Armenise et al., 2018; Badorreck et al., 2013; Bu et al., 2014; Lu et al., 2017; Yeom and Sjoblom, 2016). The thickness is the most important property of a soil crust because it directly affects evaporation, infiltration, runoff, and sediment, thereby strongly influencing soil hydrology and erosion processes. Two main methods are generally used at present for determining the thickness of physical soil crusts, i.e., direct measurement with a Vernier caliper and visual determination with a microscope (Bedaiwy, 2008; Bu et al., 2013; Hu et al., 2005b). Bedaiwy (2008) measured the thicknesses of silt loam soil and clay soil under different rainfall and runoff intensities using a Vernier caliper, and showed that the crust thickness increased as the kinetic energy of the rainfall increased. Hu et al. (2005b) observed the changes in a soil crust during the splash erosion process by using a polarized light microscope and described the characteristics of SC and DC, where the thicknesses of the two types of crust were 0.2–0.4 mm and 0.2–0.5 mm, respectively. A physical soil crust is thin and fragile, and thus it is difficult to quantify its thickness accurately, and visual observations obtained using a microscope will inevitably lead to a subjective assessment, and comparisons will be difficult between studies conducted with the same method.

In the recent decade, the use of X-ray computed tomography (CT) has developed rapidly and it has been applied widely in soil science research because of its capacity to determine the three-dimensional structure of soil in a rapid and non-destructive manner (Hu et al., 2018; Luo et al., 2008; Peyton et al., 1994; Qiao et al., 2021; Winstone et al., 2019; Zhou et al., 2017; Zhang et al., 2018). The CT technique is relatively mature for quantifying the structure of soil and it has several advantages in terms of its high resolution and objectivity for quantifying soil pores, and it can be used for determining the thickness of physical soil crusts. In particular, Bresson et al. (2004) used CT to scan slices of soil after simulated rainfall and quantified the vertical distribution of the soil bulk density (BD), thereby demonstrating the potential application of CT to quantifying the BD and crust characteristics. Hyväluoma et al. (2012) extracted the soil porosity based on CT images and determined the thickness of a soil crust as 3–4 mm to show that CT can be applied to determine the thickness of a physical soil crust. Armenise et al. (2018) used CT and a porosity threshold to determine the crust thickness for three types of soils during simulated rainfall, and analyzed the effects of the crust thickness on the soil water repellency and unsaturated hydraulic conductivity. These previous studies demonstrated that CT combined with an appropriate porosity threshold criterion can be used to determine the thickness of physical soil crusts in an objective and highly comparable manner. However, previous studies mostly focused on SCs formed on disturbed soils,

which are not representative of the actual conditions for natural bare soils, and the SC and DC were also not distinguished.

The southern red soil region is one of the main areas affected by water erosion in China. The soil in this region is highly acidic, relatively poor in nutrients, and its resistance to erosion is weak due to the specific parent material and climatic conditions. Soils that originate from granite (granite red soil, GRS) and Quaternary red clay (QRC) are typical erosive soils in this region (Deng et al., 2019; Zhu et al., 2021a; Zhu et al., 2021b). Both soils will form physical soil crusts after continuous rainfall according to actual observations but quantitative standards are lacking for characterizing these crusts. The effects of the crust thickness on the runoff and sediment yield for these two soils are also not understood. Therefore, the objectives of this study were: (1) to extract the pores in surface soil samples of GRS and QRC and analyze their spatial distribution using CT, (2) to quantify the thickness of SC and DC for GRS and QRC based on the pore distribution and threshold values, and (3) to determine the effect of the crust thickness on the runoff and sediment yield preliminary.

2. Materials and methods

2.1. Experimental site

The study was performed in the red soil region of southern China (Figure 1a) and experiments were conducted at the Red Soil Ecological Experimental Station in Yingtan city. The GRS was collected from Ganxian district, Ganzhou city, Jiangxi Province, which belongs to a subtropical monsoon humid climate zone, with an average annual temperature of 19.3°C and average annual rainfall of 1076 mm, 47.5% of which falls from April to June. The topography of this area is dominated by low mountains and hills, and most of the soils developed from granite and metamorphic rocks. The granite-derived soil is characterized by high sandiness and poor shear resistance, and collapsed gullies readily form with severe soil erosion (Deng et al., 2019). The QRC was collected from Yujiang district, Yingtan city, Jiangxi Province, which belongs to a subtropical monsoon climate zone, with an average annual temperature of 17.8°C and average annual rainfall of 1800 mm, half of which falls from April to June. The terrain in this area is dominated by low hills, but severe soil erosion is present due to the high land use efficiency, low soil fertility, poor soil structure, and abundant and concentrated rainfall (Gao et al., 2020).

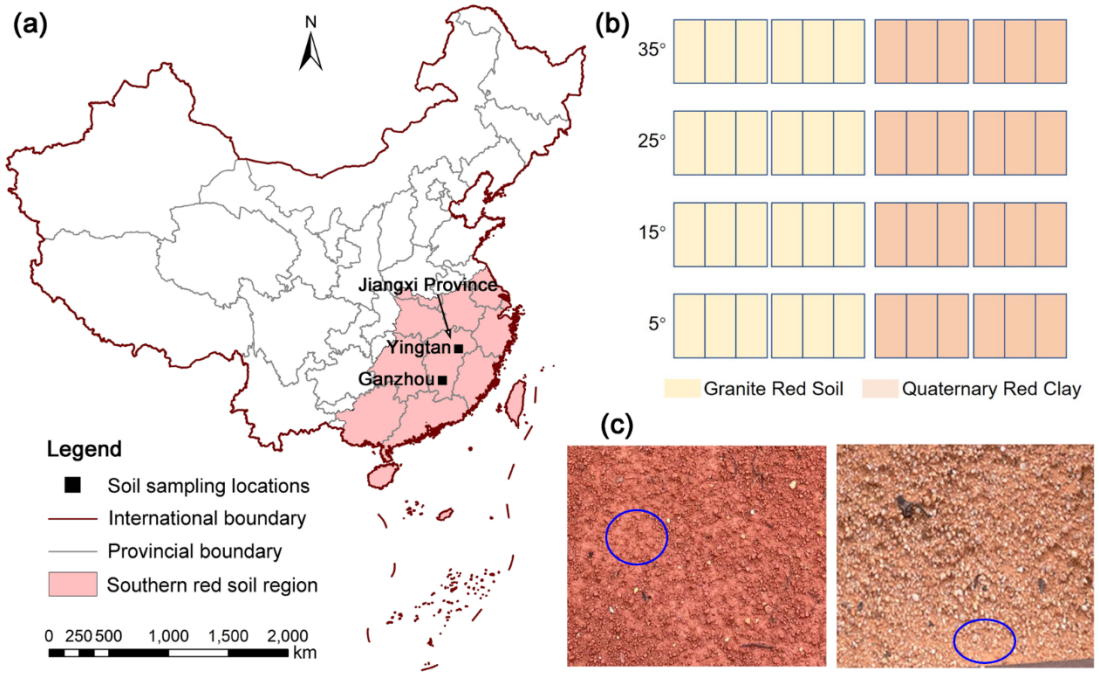

FIGURE 1 Location of the study region and sampling sites (a), layout of the experiment (b), and photographs of soil structural crust (left) and depositional crust (right) (c).

The basic properties of the GRS and QRC differed due to the parent materials and the environments where they developed (Table 1). Both the soils were acidic with low organic matter and nutrient contents. The textures of the two soils were also different. GRS had a high sand content (> 60%) and it was sandy loam according to the international soil texture classification standard. QRC had a relatively uniform particle content, with sand, silt, and clay contents of slightly more than 30%, and it was classified as clay loam.

TABLE 1 Basic properties of the granite red soil (GRS) and Quaternary red clay (QRC) at a depth of 20 cm

	Sand (%)	Silt (%)	Clay (%)	SOM (g kg^{-1})	pH	TN (g kg^{-1})	TP (g kg^{-1})	TK (g kg^{-1})
GRS	67.64	26.98	5.38	1.85	5.48	0.05	0.20	13.12
QRC	30.70	33.06	36.24	6.27	4.52	0.44	0.27	11.98

SOM, soil organic matter; TN, total nitrogen; TP, total phosphorus; TK, total potassium.

2.2. Experimental design and soil sample collection

Forty-eight micro-runoff plots were established at the red soil station, with a projection area of 1 m × 2 m. Four slopes, i.e., 5°, 15°, 25°, and 35°, were prepared according to the topographical conditions at the two sites. GRS and QRC were used to fill the plots, with six replicates per slope (Figure 1b). GRS was collected from Jingouxing watershed in Ganxian, where the soil was excavated to a depth of 50 cm with an excavator and transported to the red soil station. QRC was collected from a typical eroded area of sloped farmland at the eastern part of the station. A perforated iron sheet was placed at the bottom of the plot to allow water to soak away and a layer of gauze covered the iron sheet to prevent the loss of soil particles. The plot was then filled with soil in layers to a depth of 50 cm. A V-shaped collection trough was installed at the front end of each plot and the notch went into a plastic collection bucket with a cover to allow the collection of runoff and sediment.

In May 2021, the runoff plot experienced multiple days of rainfall, and the runoff and sediment yield were measured after the rainfall. During sampling, the water and sediment in the bucket were stirred with a wooden stick and samples were collected in a 500 mL plastic bottle. In total, 48 runoff and sediment samples were collected. The runoff and sediment were separated in the laboratory using the drying/weighing method, and the runoff and sediment yields from the micro-plot were calculated by considering the volume in the runoff bucket. It is should be noted that there was a small amount of sediment deposited at the bottom of the micro-plot due to the sidewall effect, and forming a depositional soil crust or "structure-deposition" crust (Figure 1c, right). The sediment in the bottom of the plot was small compared with the sediment yield of the whole rainfall, and it can be considered that the sediment collected from the runoff bucket can represent the actual sediment yield of the runoff micro-plot.

After collecting the runoff and sediment samples, the GRS and QRC slopes were selected at each slope gradient and a typical SC was determined in the middle part of the selected slope, before collecting an undisturbed SC soil sample using a polyvinyl chloride cutting ring with a diameter and height of 5 cm. We tried to avoid changing the shape of the surface crust when pressing down the cutting ring during the soil sampling process. Plastic film was used to wrap each sample up tightly. In order to compare with structural crusts, we also collected depositional soil crust samples at appropriate places in each plot and analyzed the pore structure characteristics. Although, most of the slopes of the plots were structural crusts, including the position of depositional crust at the beginning of the rainfall, preliminary understanding of depositional soil crust or "structure-deposition" composite crust was important to soil crust type and pore characteristic study. The same method was used to collect an undisturbed DC soil sample at the end of the plot. In total, 16 undistributed crust soil samples were collected. It should be noted that due to the high cost of scanning soil samples using the CT method, we did not repeat the samples, but instead each scanned image was cut into three small non-adjacent images in the analysis process (Figure 2a), which eliminated the influence of spatial variations in the soil properties to some extent.

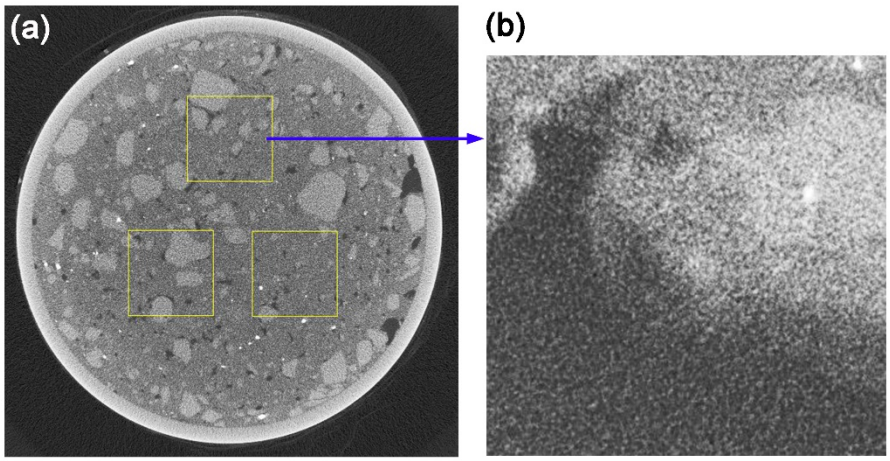

FIGURE 2 Cutting layout used for sample images (a) and example of the first image (b).

2.3. Processing and analysis of soil crust samples

An X-ray industrial CT system (GE Sensing & Inspection Technologies GmbH, Wunstorf, Germany) was used to scan the 16 undisturbed crust soil samples. The voltage was 100 kV and the current was 100 A. In total, 1700–1800 CT images were obtained for each soil sample with an image resolution of 30 m.

ImageJ (version 1.53j) software was used to extract pore information and to reconstruct the three-dimensional images. First, a region of interest (ROI) was selected and the images were then cropped based on the selected ROI. The diameter of each soil sample was 5 cm in this study. In order to eliminate the disturbance at the edge of the soil caused by the cutting ring, three squares with a side length of 10 mm were determined in the images of each soil sample, where the arrangement of the three-square ROIs is shown in Figure 2a. The average extracted porosity was treated as the porosity of the soil sample.

Air was often present between the soil crust and plastic film wrap, and the surface of the soil crust was not strictly smooth and flat, we thus needed to determine the first image at the beginning of the crust. In general, the first few scanned images were all black due to the air between the plastic wrap and the soil. The first image was selected when the air area (Figure 2b, black) and soil area (Figure 2b, off white) occupied approximately equal amounts of the image window. The height of the soil samples was 5 cm but the height of the soil column was determined as 3 cm in order to eliminate the effects of surface air and bottom soil loosening. The images that needed to be processed and analyzed were determined, i.e., from the first image to the 1000^{th} image, and they formed a cuboid with a bottom side length of 10 mm and height of 30 mm.

Image enhancement, brightness/contrast adjustment, threshold segmentation, and other operations were performed based on the ROI images. The pores and

soil structure were extracted from the binarized images generated based on an appropriate threshold value. Similar to most studies, the pore threshold value was determined according to human experience, and thus the pore threshold was not constant due to differences in the enhancement, contrast, and brightness adjustment for images of each sample. However, we ensured that the gray levels of the unselected pixels in the field of view in each sample image window were generally the same during the processing process.

2.4. Method for physical soil crust quantification

CT was used to extract the soil porosity and the thickness of the surface crust was assessed by setting a porosity threshold for the soil samples. In general, the physical soil crusts quantified by CT in previous studies had thicknesses of 0.6–5.4 mm, and actual observations in the study area also showed that the thickness of the physical crusts did not exceed 10 mm (Armenise et al., 2018; Hyväluoma et al., 2012). Therefore, we divided the soil column into two layers, where the upper crust layer measured 0–9 mm and it corresponded to scanned images 1–300, and the lower contrast layer corresponded to images 301–1000. The average porosity value for the lower layer was used as the threshold porosity to determine the thickness of the upper crust layer. The 9–30 mm layer was at a moderate distance from the crust, which eliminated the heterogeneity of the soil itself when it was far away from the crust and the impact of the crust when it was excessively close to the crust. Armenise et al. (2018) successfully quantified the thickness of three types of soils using the same method and analyzed the crust development process during simulated rainfall.

3. Results

3.1. Soil pore distribution

The three-dimensional distributions of the pores in the soil samples under different slope gradients had similar characteristics, where they generally had fine and dense spatial distributions. For example, the pore distribution in DC for QRC (Figure 3) under the four slopes was finely fragmented and dense, where the medium and small soil pores comprised a large proportion and there were almost no large pores. The changes in the soil pore distributions with depth under the four slopes were not consistent, where the soil pores clearly increased with depth in the samples from the 5° slope, whereas the pores under the other slope conditions did not exhibit significant trends with depth.

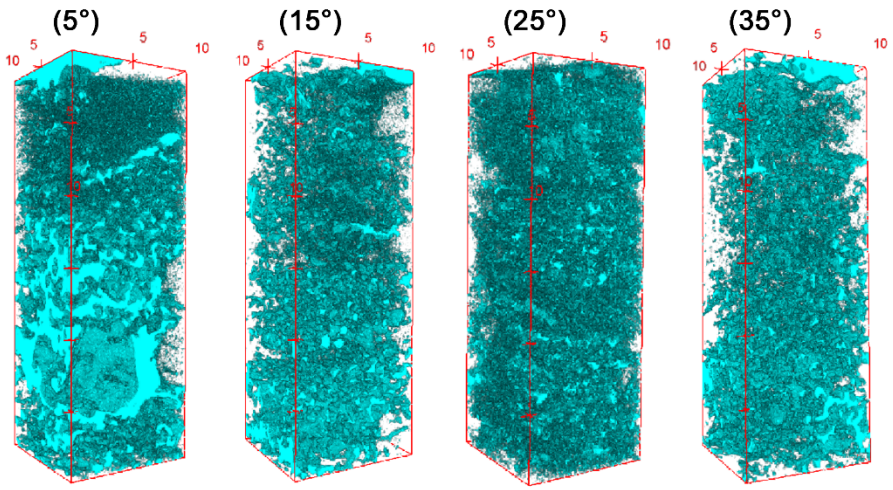

FIGURE 3 Three-dimensional distribution of soil pores in depositional crust samples from Quaternary red clay at slope gradients of 5°, 15°, 25°, and 35°.

The variations in the porosity trends in the SC and DC samples from GRS and QRC with depth were obtained by analyzing and extracting the three-dimensional pores (Figure 4). The variations in the porosity of the four soil samples followed the same trend in the 0–3 mm layer, where the porosities all tended to increase rapidly. The variations in the subsequent 3–30 mm were not exactly the same, where the porosity decreased with depth in the SC soil samples, whereas it fluctuated almost vertically in the DC soil samples. The soil porosity profile distribution differed among the slope conditions. The porosities of the SC soil samples were relatively similar under the four slopes and the four curves were relatively clustered, whereas the porosities of the DC soil samples were quite different under the four slopes and the four curves were relatively discrete. In general, the degree of dispersion of the porosity curve gradually increased with the depth.

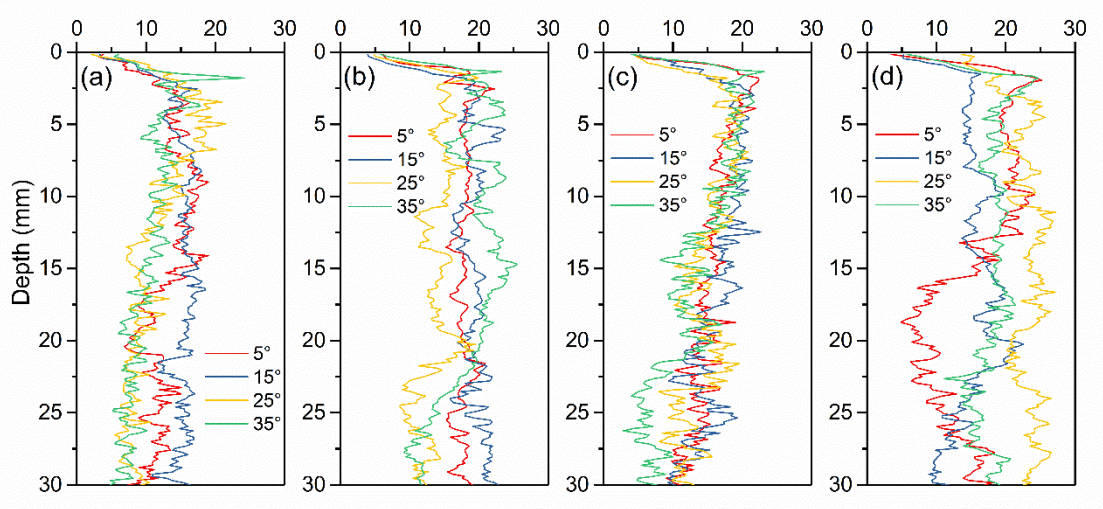

FIGURE 4 Variations in the soil porosity with depth in the structural crust sample from the granite red soil (a), depositional crust sample from the granite red soil (b), structural crust sample from the Quaternary red clay (c), and depositional crust sample from the Quaternary red clay (d).

Statistical porosity metrics were obtained for the SC and DC samples from GRS and QRC at various slopes (Table 2). The mean soil porosity was 15.47% with a range of 1.66–28.83%. The minimum value was determined for the DC sample from GRS with a slope of 25° and the maximum value for the SC sample from QRC with a slope of 25°. The median value was 15.85%, which was close to the mean, thereby indicating the normality of the porosity data. The standard deviation and coefficient of variation (CV) of the porosity were small, where their distribution was relatively clustered with moderate to weak spatial variability.

TABLE 2 Basic soil porosity (%) statistics for all samples

	Minimum	Maximum	Mean	Median	SD	CV
SG5	5.68	22.64	17.52	17.90	2.12	0.12
SG15	3.71	24.38	18.87	19.45	3.15	0.17
SG25	4.44	21.97	13.55	13.85	2.66	0.20
SG35	4.93	26.80	18.45	19.72	4.47	0.24
DG5	2.94	20.17	12.74	12.82	3.30	0.26
DG15	2.80	19.18	14.97	15.54	2.45	0.16
DG25	1.66	24.92	10.91	9.50	4.17	0.38
DG35	3.67	25.88	10.01	9.93	3.10	0.31
SQ5	2.67	25.91	15.26	16.02	5.72	0.38
SQ15	4.78	23.04	15.21	15.28	3.23	0.21
SQ25	12.08	28.83	22.88	23.39	2.88	0.13
SQ35	4.04	25.81	17.89	18.39	2.73	0.15

	Minimum	Maximum	Mean	Median	SD	CV
DQ5	3.96	23.96	15.38	15.45	3.18	0.21
DQ15	4.60	23.62	16.30	17.02	3.68	0.23
DQ25	4.35	22.39	14.57	14.98	3.69	0.25
DQ35	2.56	24.15	12.96	12.79	5.48	0.42
Total	1.66	28.83	15.47	15.85	4.79	0.31

SD, standard deviation; CV, coefficient of variation; SG, structural crust on granite red soil; DG, depositional crust on granite red soil; SQ, structural crust on Quaternary red clay; DQ, depositional crust on Quaternary red clay. Numbers after capital letters refer to the slope gradient.

The porosities of samples from different soil types (GRS and QRC) and different crust types (SC and DC) varied according to the slope gradient. The porosity of the SC sample from GRS varied little with the slope, whereas that of the SC sample from QRC increased with the slope. The porosities of the DC samples from the two soils exhibited the same trend, where both decreased with the slope. The CVs of the porosity for the SC samples from GRS and QRC exhibited opposite changes with the slope, where the CV of the porosity for the SC sample from GRS increased with the slope, whereas the CV of the porosity for the SC sample from QRC decreased with the slope. However, the trends in the CV of the porosity for the DC samples from the two soils generally varied in the same manner with the slope, where they tended to increase with the slope, and thus the spatial variability in the porosity of the DC samples was higher when the slope gradient was greater.

The porosities of the two crust types also clearly differed, where the minimum, maximum, average, and median porosity were generally greater for the SC samples than those for the DC samples, where they reflected the compactness of the DC sample and relatively loose structure of the SC samples, and these results are consistent with the dense and scattered pore distribution in the SC soil samples shown in Figure 3.

3.2. Thickness of physical soil crusts

Table 3 shows the thicknesses of SC and DC from GRS and QRC at various slope gradients. The mean thickness of the crusts on all of the soil samples was 1.31 mm, with a minimum value of 0.60 mm for SC from GRS with a slope of 25° and a maximum value of 3.09 mm for the DC from QRC with a slope of 25°.

TABLE 3 Thickness of structural crust (SC, mm) and depositional crust (DC, mm) on granite red soil (GRS) and Quaternary red clay (QRC) at various slopes

	GRS				QRC			
	5°	15°	25°	35°	5°	15°	25°	35°

	GRS		QRC					
SC	1.68	2.40	0.60	0.78	0.72	1.20	1.38	0.48
DC	1.05	1.83	1.08	1.20	0.66	1.38	3.09	1.41

The thicknesses of the soil crusts varied among the different soil types, crust types, and slope gradients (Figure 5). The thicknesses of SC and DC differed with the slope under the same soil type (Figures 5a and 5b). The thickness of SC for GRS generally decreased with the slope but the thickness of DC changed little. The thickness of SC for GRS was higher than that of DC under gentle slopes (i.e., 5° and 15°) but the opposite was found at large slopes (i.e., 25° and 35°). The thickness of SC for QRC generally increased with the slope, while the variation in the thickness of DC with the slope was generally stable. The thicknesses of DC for QRC were larger than those of SC at various slopes, and the difference increased with the slope. The crust thickness varied with the slope even for the same crust type due to the different soil type (Figures 5c and 5d). The thickness of SC for GRS decreased with the slope, whereas the thickness of SC for QRC changed little. Except for the slope gradient of 25°, the thicknesses of SC for GRS were all larger than those for QRC at the other slope gradients, thereby indicating that the SC formed more readily on GRS compared with QRC. The thickness of DC for GRS changed little with the slope, whereas the thickness of DC for QRC increased with the slope. Under gentle slopes, the thicknesses of the DC for GRS were similar to those for QRC. However, under large slopes, the thicknesses of DC for QRC were larger than those for GRS, thereby indicating that the influence of the slope on the formation of SC and DC varied between the two soils.

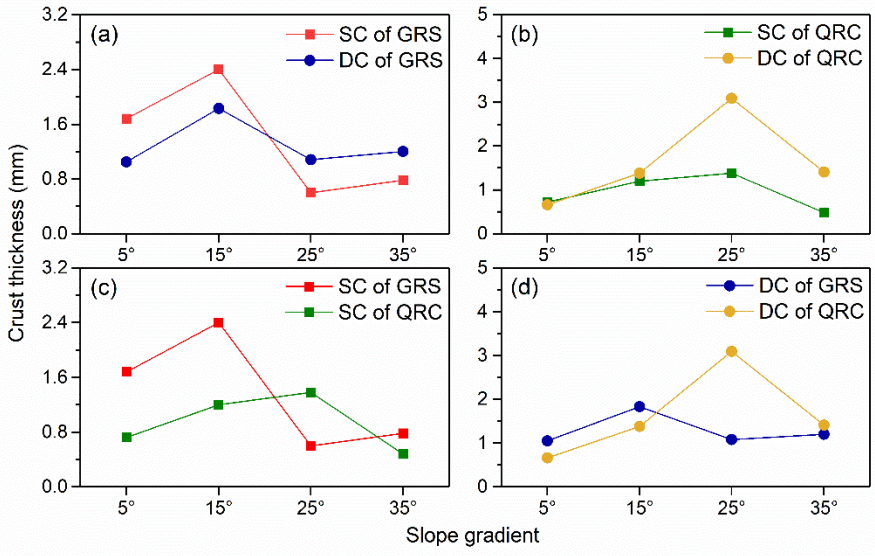

FIGURE 5 Thickness of structural crusts on granite red soil (SG) and Quaternary red clay (SQ), and depositional crust on granite red soil (DG) and Quaternary red clay (DQ) at various slope gradients.

3.3. Runoff and sediment yield, and their relationships with crust thickness

We detected clearly different trends in the runoff and sediment yields for the different micro-plot slopes with GRS and QRC (Figure 6). The runoff yield for GRS decreased with the slope, where the runoff yield decreased by 36.3% as the slope increased from 5° to 35°. The runoff yield for QRC decreased initially and then increased with the slope, where the runoff yield decreased by 50.8% as the slope gradient increased from 5° to 25°. The variation in the sediment yields from the two soils with the slope followed the opposite trend to that in the runoff. The sediment yield for GRS increased with the slope, where the sediment yield increased 1.34 times as the slope gradient increased from 5° to 35°, but the sediment yield for QRC increased initially and then decreased with the slope.

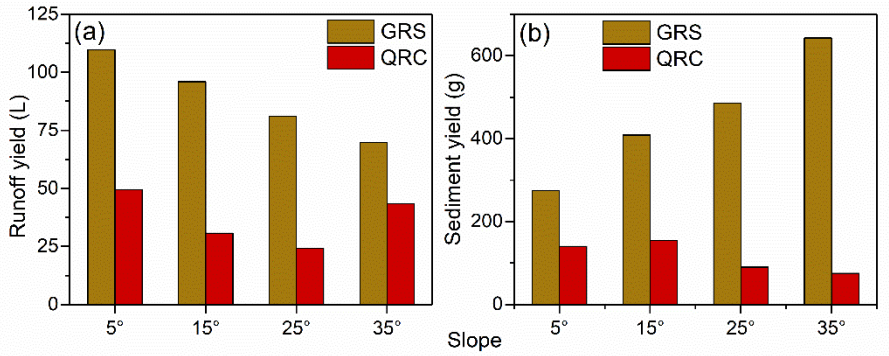

FIGURE 6 Runoff (a) and sediment yields (b) for the granite red soil (GRS) and Quaternary red clay (QRC) with different slopes.

The results of runoff and sediment measurement represented the runoff and sediment yield of the micro-plot slope, and most of the surface soil of the slope developed SC, therefore relationship between structural soil crust and slope runoff and sediment yield can be analyzed preliminarily. Results show that SC has different effects on runoff and sediment yield of the slope (Figure 7). The runoff yield of the slope had a positive relationship with SC thickness, i.e. runoff yield increased with the increase of SC crust thickness. The sediment yield also increased with SC thickness, but the trend was not significant.

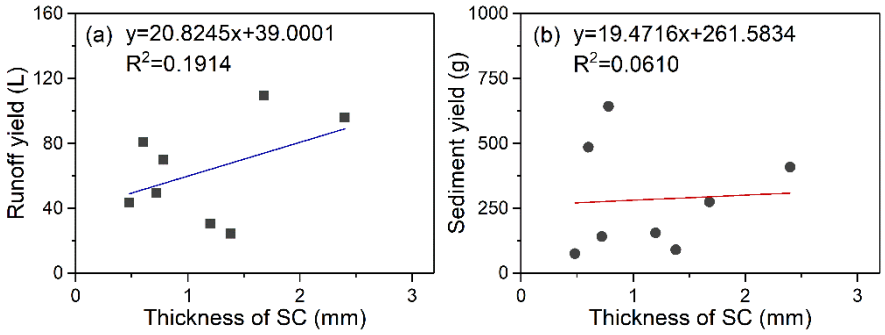

FIGURE 7 Relationships between structural crust (SC) with runoff and sediment yield.

4. Discussion

4.1. Crust thickness and its quantification

According to the present study, the mean physical soil crust thickness was 1.31 mm with a range of 0.6–3.09 mm. This result is comparable with the results obtained by Tackett and Pearson (1965) and Armenise et al. (2018) who determined crust thicknesses of 1–3 mm and 0.6–5.4 mm, respectively. However, the physical soil crust thicknesses determined in most studies were higher than those in our study. For example, the crust thickness was determined as 1–8 mm by Bu et al. (2013), 0.6–16.8 mm by Bedaiwy (2008), < 6 to 8 mm by Fohrer et al. (1999), and 4 mm by Hyväluoma et al. (2012). The formation of a physical soil crust is mainly related to the soil texture and physical properties, where crusts are more likely to form on silty loam compared with clay loam (Bedaiwy, 2008). Soils with a low organic matter content and low water stable aggregate content usually exhibit poor cohesion and they readily form crusts (Armenise et al., 2018).

Excluding the studies by Armenise et al. (2018), Fohrer et al. (1999), and Hyväluoma et al. (2012), most previous studies of physical soil crust thickness used the direct measurement method with a Vernier caliper or visual measurement method based on light microscopy or electron microscopy, thereby leading to errors caused by human subjective judgments and increased variability in the crust thickness. The method used to determine the physical soil crust thickness in the present study is based on CT image analysis and porosity threshold determination, and it can be employed to objectively quantify the crust thickness, thereby facilitating comparisons of the crust thickness in different studies. Similarly, Fohrer et al. (1999) scanned crust soil samples using medical CT, and extracted and analyzed the BD distribution with depth. Hyväluoma et al. (2012) quantified the physical crust thickness for different soil types with CT and concluded that CT could be used for quantifying the thickness of physical soil crusts after determining appropriate soil indicators. Armenise et al. (2018) used the mean soil porosity in the lower contrast layer of soil samples as the

threshold value to characterize the crust development process under simulated rainfall, and its effects on the soil physics and hydrological dynamics. Therefore, it is feasible to determine the crust thickness using CT with an appropriate porosity threshold.

4.2. Effects of soil type and slope on crust

The crust thickness is strongly influenced by the soil properties. In the present study, the average crust thickness for GRS was 1.33 mm and it was higher than that for QRC (1.29 mm). In particular, the average thickness of SC for GRS was 1.37 mm and it was 1.44 times that for QRC because GRS was a sandy loam with high sand and silt contents and low clay content, whereas QRC was a clay loam with a high clay content. In addition, the organic matter content of GRS was low at only 30% (Table 1). Studies have shown that soils with low clay, organic matter, and water stable aggregate contents are likely to be splashed and separated to fill the pores of the topsoil due to the relatively small interaction force between the soil particles, and thus they readily form a physical soil crust (Bedaiwy, 2008; Hu et al., 2005a). The average thickness of SC for GRS was higher than that for QRC, but the average thickness of DC for GRS (1.29 mm) was smaller than that for QRC (1.64 mm), thereby indicating that the soil type specifically affected the thickness of the different crust types. SC was formed by raindrops splashing and filling the soil pores with fine particles and raindrop compaction. DC was formed by the deposition of fine particles in runoff on a gentle slope. The two crust types were formed by different mechanisms, and thus their characteristic responses varied according to the different soil types (Badorreck et al., 2013; Hu et al., 2005b; Lu et al., 2017).

The slope was an important factor that affected the crust thickness, but the effect varied among the different soil and crust types. In particular, the thicknesses of SC for GRC and QRC decreased with the slope, whereas the thickness of DC for QRC increased with the slope (Figure 5), mainly because the SC was formed by the impact of raindrops, so when the slope was greater, the component force of gravity perpendicular to the slope was weaker and the soil crust thickness was smaller (Assouline, 2004; Fox et al., 1997). DC was formed by the accumulation of sediment particles carried by runoff, which were mainly related to the sediment carrying capacity and runoff yield. The runoff and sediment yield were generally higher with a larger slope, and thus the sediment deposited at the end of the micro-plot and the thickness of the DC were larger (Fox et al., 1997; Hu et al., 2005b; Lu et al., 2017).

4.3. Runoff and sediment characteristics and its slope influencing factors

The runoff yields for GRS and QRC decreased with slopes ranging from 5–25°, but different results were obtained in most previous studies in the same study area, which showed that the runoff yield generally increased with the slope, or an inflection point was determined for the slope where the runoff increased before the inflection point and decreased after it (Han et al., 2021; Jourgholami et al., 2021; Shen et al., 2016). Other studies also showed that the runoff yield

decreased with the slope but the reason for the decrease was considered to be the reduction in the rain carrying capacity due to the reduced projected area of the slope as the slope gradient increased under simulated rainfall (Liang et al., 2017; Zhang et al., 2009). Zhang et al. (2009) studied the influence of the slope gradient on the erosion of red soil in the same study region under simulated rainfall by using a micro-plot with an adjustable slope and found that the runoff decreased by 22.3% as the slope gradient increased from 5° to 25°, where this decrease was considered to be mainly due to the reduced rain carrying capacity. However, it should be noted that when the slope increased from 5° to 25°, the rainfall carrying capacity of the micro-plot only decreased by 9.02%, which was smaller than the decrease in the runoff yield. Under a specific rainfall intensity, the runoff yield is only affected by the soil infiltration characteristics and the rainfall carrying capacity of the slope. However, in the present study, the rainfall carrying capacity was constant because the projected area was the same in the micro-plots. Thus, the differences in the infiltration characteristics mainly explained the decrease in the runoff with the slope. The following three main reasons may explain the changes in the soil infiltration characteristics with the slope. (1) Under the same rainfall, the initial rainfall more readily removed the fine particles and left more coarse soil particles on the slope as the slope gradient increased, thereby leading to increased infiltration (Deng et al., 2018). (2) The degree of soil erosion varies among different slopes, thereby leading to variations in the micro-topography formed. Soil on greater slopes often undergoes severe erosion with relatively high surface roughness, which increases the resistance to runoff and promotes runoff infiltration to some extent (Jiang et al., 2018a). (3) According to our actual observations, physical soil crusts formed on GRS and QRC under continuous rainfall with various slopes (Table 3), thereby affecting water infiltration, but the different slopes had diverse effects on crust formation, and thus the slope also influenced the decrease in the runoff with the slope.

Physical soil crusts can affect the runoff and sediment yield. In the present study, both the runoff and sediment yields increased with the thickness of SC (Figure 7), because the SC had a large area of the experimental plot, where the runoff infiltration decreased as the thickness of SC increased, and the runoff and sediment yield increased in the plots. Armenise et al. (2018), Assouline and Mualem, (2006) and Jiang et al. (2018b) also showed that increases in the crust thickness decreased water infiltration and increased the runoff and soil erosion risk. The effect of physical soil crust on the water and sediment behavior of slopes cannot be ignored, and understanding the impact of soil physical crusts on runoff and sediment process and yield on slopes with different gradients plays an important role in slope erosion mechanism research and erosion management.

5. Conclusions

In the present study, we used CT to extract the soil porosity and quantified the thickness of two types of physical crusts on two typical erosive soils in southern China. We analyzed the contribution of the soil crust to the runoff and

sediment yields based on runoff and sediment yield measurements obtained from experimental micro-plots. The CT method reproduced the internal structure of the soil by tomographic scanning, and it had the advantages of providing an intuitive visualization and objectively quantifying the soil pore distribution. This method allowed the objective quantification of the crust thickness on soil by taking the average soil porosity of the lower layer (9–30 mm) of the sample as an assessment threshold in order to determine the thickness of the physical soil crust. The soil type and slope had important effects on soil crust formation under the same rainfall conditions, where silt loam more readily formed a crust compared with clay loam due to the low organic matter content, where the thickness of the SC was smaller and that of the DC was larger when the slope gradient was greater. Physical soil crusts affected the runoff and sediment yield by changing the slope infiltration conditions, and the thicknesses of SC of the two soils changed differently with the slope in the present study, thereby partly explaining the abnormal changes in the runoff and sediment yield with the slope. Thus, in the present study, we used a new method to quantify the thickness of physical crusts that formed on two soils from southern China and analyzed their impacts on the runoff and sediment yield. This method may provide new insights into the mechanisms responsible for erosion and facilitate soil erosion management in the red soil region of China.

References

Armenise, E., Simmons, R.W., Ahn, S., Garbout, A., Doerr, S.H., Mooney, S.J., Sturrock, C.J., & Ritz, K. (2018). Soil seal development under simulated rainfall: Structural, physical and hydrological dynamics. *Journal of Hydrology*, *556*, 211-219.

Assouline, S. (2004). Rainfall-induced soil surface sealing: A critical review of observations, conceptual models, and solutions. *Vadose Zone Journal*, *3*(2), 570-591.

Assouline, S., & Mualem, Y. (2006). Runoff from heterogeneous small bare catchments during soil surface sealing. *Water Resources Research*, *42*(12).

Badorreck, A., Gerke, H.H., & Hüttl, R.F. (2013). Morphology of physical soil crusts and infiltration patterns in an artificial catchment. *Soil & Tillage Research*, *129*, 1-8.

Bedaiwy, M.N.A. (2008). Mechanical and hydraulic resistance relations in crust-topped soils. *Catena*, *72*(2), 270-281.

Bresson, L.M., Moran, C.J., & Assouline, S. (2004). Use of bulk density profiles from X-radiography to examine structural crust models. *Soil Science Society of America Journal*, *68*(4), 1169-1176.

Bu, C.F., Gale, W.J., Cai, Q.G., & Wu, S.F. (2013). Process and mechanism for the development of physical crusts in three typical Chinese soils. *Pedosphere*, *23*(3), 321-332.

Bu, C.F., Wu, S.F., & Yang, K.B. (2014). Effects of physical soil crusts on infiltration and splash erosion in three typical Chinese soils. *International Journal of Sediment Research*, *29*(4), 491-500.

Chamizo, S., Cantón, Y., Miralles, I., & Domingo, F. (2012). Biological soil crust development affects physicochemical characteristics of soil surface in semiarid ecosystems. *Soil Biology & Biochemistry*, *49*, 96-105.

Deng, L.Z., Zhang, L.P., Fan, X.J., Wu, Y.H., Sun, T.Y., & Fei, K. (2018). Characteristics of runoff and sediment yield under different rainfall intensities and slope gradients in erosive weathered granite area. *Transactions of the CSAE*, *34*(17), 143-150.

Deng, Y., Shen, X., Xia, D., Cai, C., Ding, S., & Wang, T. (2019). Soil Erodibility and Physicochemical Properties of Collapsing Gully Alluvial Fans in Southern China. *Pedosphere*, *29*(1), 102-113.

Fohrer, N., Berkenhagen, J., Hecker, J.M., & Rudolph, A. (1999). Changing soil and surface conditions during rainfall - Single rainstorm/subsequent rainstorms. *Catena*, *37*(3-4), 355-375.

Fox, D.M., Bryan, R.B., & Price, A.G. (1997). The influence of slope angle on final infiltration rate for interrill conditions. *Geoderma*, *80* (1-2), 181-194.

Gao, L., Bowker, M.A., Xu, M., Sun, H., Tuo, D., & Zhao, Y. (2017). Biological soil crusts decrease erodibility by modifying inherent soil properties on the Loess Plateau, China. *Soil Biology & Biochemistry*, *105*, 49-58.

Gao, L., Peng, X., & Biswas, A. (2020). Temporal instability of soil moisture at a hillslope scale under subtropical hydroclimatic conditions. *Catena*, *187*.

Han, D., Deng, J., Gu, C., Mu, X., Gao, P., & Gao, J. (2021). Effect of shrubgrass vegetation coverage and slope gradient on runoff and sediment yield under simulated rainfall. *International Journal of Sediment Research*, *36*(1), 29-37.

Hu, X., Cai, Q.G., Liu, L.Y., Cai, C.F., Li, S.J., & Zhu, D.Y. (2005a). Development of soil crust through simulated rainfall in laboratory. *Acta Pedologica Sinica*, *42*(03), 504-507.

Hu, X., Li, Z., Li, X., Wang, P., Zhao, Y., Liu, L., & Lü, Y. (2018). Soil Macropore Structure Characterized by X-Ray Computed Tomography Under Different Land Uses in the Qinghai Lake Watershed, Qinghai-Tibet Plateau. *Pedosphere*, *28*(3), 478-487.

Hu, X., Yan, P., Li, S.J., Cai, Q.G., Liu, L.Y., Cai, C.F., Zhu, Y.D., & Zhang, G.Y. (2005b). Development of soil crust through rainfall simulating in laboratory and relationship between crust and splash erosion. *Journal of Soil and Water Conservation*, *19*(02), 13-16.

Hyväluoma, J., Thapaliya, M., Alaraudanjoki, J., Sirén, T., Mattila, K., Timonen, J., & Turtola, E. (2012). Using microtomography, image analysis and

flow simulations to characterize soil surface seals. *Computers & Geosciences*, *48*, 93-101.

Jiang, F., Zhan, Z., Chen, J., Lin, J., Wang, M.K., Ge, H., & Huang, Y. (2018a). Rill erosion processes on a steep colluvial deposit slope under heavy rainfall in flume experiments with artificial rain. *Catena*, *169*, 46-58.

Jiang, Z.Y., Li, X.Y., Wei, J.Q., Chen, H.Y., Li, Z.C., Liu, L., & Hu, X. (2018b). Contrasting surface soil hydrology regulated by biological and physical soil crusts for patchy grass in the high-altitude alpine steppe ecosystem. *Geoderma*, *326*, 201-209.

Jourgholami, M., Karami, S., Tavankar, F., Lo Monaco, A., & Picchio, R. (2021). Effects of Slope Gradient on Runoff and Sediment Yield on Machine-Induced Compacted Soil in Temperate Forests. *Forests*, *12*(1).

Liang, Z.Q., Zhang, S.Y., Zhuo, M.N., Xie, Z.Y., Liao, Y.S., & Li, D.Q. (2017). Effects of rainfall intensity and slope gradient on erosion process in red soil hillslopes. *Bulletin of Soil and Water Conservation*, *37*(02), 1-6.

Liu, F., Zhang, G.H., Sun, L., & Wang, H. (2016). Effects of biological soil crusts on soil detachment process by overland flow in the Loess Plateau of China. *Earth Surface Processes and Landforms*, *41*(7), 875-883.

Lu, P., Xie, X., Wang, L., & Wu, F. (2017). Effects of different spatial distributions of physical soil crusts on runoff and erosion on the Loess Plateau in China. *Earth Surface Processes and Landforms*, *42*(13), 2082-2089.

Luo, L., Lin, H., & Halleck, P. (2008). Quantifying soil structure and preferential flow in intact soil using X-ray computed tomography. *Soil Science Society of America Journal*, *72*(4), 1058-1069.

Peyton, R.L., Gantzer, C.J., Anderson, S.H., Haeffner, B.A., & Pfeifer, P. (1994). Fractal dimension to describe soil macropore structure using X-ray computed-tomography. *Water Resources Research*, *30*(3), 691-700.

Qiao, J., Liu, X., Zhu, Y., Jia, X., & Shao, M. (2021). Three-dimensional quantification of soil pore structure in wind-deposited loess under different vegetation types using industrial X-ray computed tomography. *Catena*, *199*.

Rodríguez-Caballero, E., Cantón, Y., & Jetten, V. (2015). Biological soil crust effects must be included to accurately model infiltration and erosion in drylands: An example from Tabernas Badlands. *Geomorphology*, *241*, 331-342.

Shen, H., Zheng, F., Wen, L., Han, Y., & Hu, W. (2016). Impacts of rainfall intensity and slope gradient on rill erosion processes at loessial hillslope. *Soil & Tillage Research*, *155*, 429-436.

Tackett, J.L., & Pearson, R.Q. (1965). Some characteristics of soil crusts formed by simulated rainfall. *Soil Science*, *99*, 7.

Winstone, B.C., Heck, R.J., Munkholm, L.J., & Deen, B. (2019). Characterization of soil aggregate structure by virtual erosion of X-ray CT imagery. *Soil & Tillage Research*, *185*, 70-76.

Wu, Q., Wang, L., & Wu, F. (2016). Effects of structural and depositional crusts on soil erosion on the Loess Plateau of China. *Arid Land Research and Management*, *30*(4), 432-444.

Yeom, S., & Sjoblom, K. (2016). Structural soil crust development from raindrop impacts using two-dimensional discrete element method. *Computer & Geoscience*, *97*, 49-57.

Zhang, H.R., Zheng, F.L., & Geng, X.D. (2009). Effect of slope gradients on soil erosion process in red earth hillslopes. *Research of Soil and Water Conservation*, *16*(04), 52-54, 59.

Zhang, Z., Liu, K., Zhou, H., Lin, H., Li, D., & Peng, X. (2018). Three dimensional characteristics of biopores and non-biopores in the subsoil respond differently to land use and fertilization. *Plant and Soil*, *428*(1-2), 453-467.

Zhou, H., Mooney, S.J., & Peng, X. (2017). Bimodal Soil Pore Structure Investigated by a Combined Soil Water Retention Curve and X-Ray Computed Tomography Approach. *Soil Science Society of America Journal*, *81*(6).

Zhu, X., Liang, Y., Tian, Z., & Wang, X. (2021a). Analysis of scale-specific factors controlling soil erodibility in southeastern China using multivariate empirical mode decomposition. *Catena*, *199*, 10.

Zhu, X., Liang, Y., Tian, Z., Zhang, Y., Zhang, Y., Du, J., Wang, X., Li, Y., Qu, L., & Dai, M. (2021b). Simulating soil erodibility in southeastern China using a sequential Gaussian algorithm. *Pedosphere*, *31*(5), 715-724.